EBioMedicine 16 (2017) 292–301

Contents lists available at ScienceDirect

EBioMedicine

journal homepage: www.ebiomedicine.com

Research Paper

# Glutaminolysis is Essential for Energy Production and Ion Transport in Human Corneal Endothelium

Wenlin Zhang [a,*], Hongde Li [b], Diego G. Ogando [a], Shimin Li [a], Matthew Feng [c], Francis W. Price Jr [c], Jason M. Tennessen [b], Joseph A. Bonanno [a,*]

[a] School of Optometry, Indiana University, Bloomington, IN 47405, USA
[b] Department of Biology, Indiana University, Bloomington, IN 47405, USA
[c] Price Vision Group, Indianapolis, IN 46260, USA

ARTICLE INFO

*Article history:*
Received 19 October 2016
Received in revised form 3 January 2017
Accepted 4 January 2017
Available online 13 January 2017

*Keywords:*
Glutaminolysis
Energy metabolism
Corneal endothelium
SLC4A11 ammonia transporter
Congenital hereditary endothelial dystrophy (CHED)
Fuchs' endothelial corneal dystrophy (FECD)

ABSTRACT

Corneal endothelium (CE) is among the most metabolically active tissues in the body. This elevated metabolic rate helps the CE maintain corneal transparency by its ion and fluid transport properties, which when disrupted, leads to visual impairment. Here we demonstrate that glutamine catabolism (glutaminolysis) through TCA cycle generates a large fraction of the ATP needed to maintain CE function, and this glutaminolysis is severely disrupted in cells deficient in $NH_3$:$H^+$ cotransporter Solute Carrier Family 4 Member 11 (SLC4A11). Considering SLC4A11 mutations leads to corneal endothelial dystrophy and sensorineural deafness, our results indicate that SLC4A11-associated developmental and degenerative disorders result from altered glutamine catabolism. Overall, our results describe an important metabolic mechanism that provides CE cells with the energy required to maintain high level transport activity, reveal a direct link between glutamine metabolism and developmental and degenerative neuronal diseases, and suggest an approach for protecting the CE during ophthalmic surgeries.

© 2017 The Authors. Published by Elsevier B.V. This is an open access article under the CC BY-NC-ND license (http://creativecommons.org/licenses/by-nc-nd/4.0/).

## 1. Introduction

The Corneal Endothelium (CE) is a cell monolayer on the posterior surface of the cornea that is essential for maintaining corneal hydration, thickness, and transparency. CE is one of the most metabolically active tissues in the body with the highest mitochondrial density, second only to photoreceptors (Hogan et al., 1971), and corneal endothelial dystrophies are the most common indication for corneal transplants worldwide (Dorrepaal et al., 2007; Ghosheh et al., 2008). One major function of CE is to generate an outward osmotic driving force that counteracts an inward imbibition pressure generated by corneal stromal glycosaminoglycans (Barfort and Maurice, 1974). Maintenance of the osmotic force is dependent on primary active transport ($Na^+$-$K^+$-ATPase activity) and numerous secondary membrane ion transporters (Bonanno, 2012; Geroski and Edelhauser, 1984; Li et al., 2016). Together this is generally referred to as the CE pump function. Failure of the CE pump results in corneal swelling, loss of transparency, and in turn, visual impairment.

The robust ion and fluid transport activity of the CE imposes heavy metabolic demands on these cells (Bourne, 2003). Consistent with this, in addition to having a high mitochondrial density, CE dysfunction is a common symptom associated with mitochondrial disorders, such as Pearson Syndrome, Kearns-Sayre syndrome and Leigh's syndrome (Boonstra et al., 2002; Chang et al., 1994; Hayashi et al., 2000; Kasbekar et al., 2013). However, despite the intense energetic demands imposed by the CE pump function, the metabolic mechanisms required for maintaining high levels of energy remain largely unexplored. In this regard, understanding CE metabolism is of particular interest for cataract surgeries and corneal transplants, as CE pump function may be impaired for a time following these procedures, resulting in visually significant corneal edema. Currently, there is no way to clinically restore or augment CE pump function. Therefore, metabolic therapies that maximize available energy represent a potential means to improve CE pump function and surgical outcomes.

The membrane transporter *SLC4A11* has recently emerged as an important player in CE pump function. Not only is this gene highly expressed in the CE (Chng et al., 2013), but mutations in *SLC4A11* also cause a collection of developmental and/or degenerative corneal disorders such as Congenital Hereditary Endothelial Dystrophy (CHED), Harboyan Syndrome, Fuchs Endothelial Corneal Dystrophy (FECD), and Peters anomaly (Siddiqui et al., 2014; Vithana et al., 2006, 2008; Weh et al., 2014), as well as sensorineural deafness (Harboyan Syndrome,

* Corresponding authors.
*E-mail addresses:* wenlzhan@indiana.edu (W. Zhang), jbonanno@indiana.edu (J.A. Bonanno).

http://dx.doi.org/10.1016/j.ebiom.2017.01.004
2352-3964/© 2017 The Authors. Published by Elsevier B.V. This is an open access article under the CC BY-NC-ND license (http://creativecommons.org/licenses/by-nc-nd/4.0/).

CHED plus perceptive deafness) (Siddiqui et al., 2014). Intriguingly, SLC4A11 was recently found to function as an $NH_3$:$2H^+$ co-transporter (Zhang et al., 2015), indicating that ammonia metabolism plays an unexpected role in CE development, function, and degeneration. Since ammonia is a common waste product of amino acid catabolism, especially glutamine (Yang et al., 2009), these observations suggest that the CE may actively use glutamine to maintain $Na^+$-$K^+$-ATPase activity. In addition, the steady-state concentration of glutamine in human aqueous humor (0.6–0.8 mM) (Langford et al., 2007) is similar to plasma, further supporting the potential for glutamine metabolism.

Here we use rabbit, mouse, and human CE to investigate the link between CE metabolism and ammonia production. Strikingly, our findings reveal that the CE produces ammonia due to high levels of glutaminolysis. However, unlike stem cells and cancer cells that use glutamine to support biosynthesis (Le et al., 2012), we demonstrate that the non-proliferating CE uses glutamine to produce ATP for $Na^+$-$K^+$-ATPase activity to support physiological pump function. And this glutaminolysis is disrupted in SLC4A11 transporter deficient CE resulting in inhibition of pump function and significant pathology. This work sheds light on clinical metabolic therapies to facilitate CE function, pathogenesis of CHED, FECD and Harboyan syndrome, and suggest that the ammonia handling capacity offered by $NH_3$:$H^+$ transporter SLC4A11 is essential for cells actively metabolizing glutamine.

## 2. Materials and Methods

### 2.1. Animals

All mice were housed and maintained in pathogen-free conditions and used in the experiments in accordance with institutional guidelines and the current regulations of the National Institutes of Health, the United States Department of Health and Human Services, the United States Department of Agriculture and Association for Research in Vision and Ophthalmology (ARVO) Statement for the Use of Animals in Ophthalmic and Vision Research.

### 2.2. RNA Extraction

Total RNA, from human corneal endothelial tissue, mouse endothelial tissue, immortalized HCEC cell line, and FECD patient corneal endothelial tissue were extracted and purified via RNeasy mini kit (#74104, Qiagen) with DNase digestion (#79254, Qiagen).

Healthy human corneal endothelium: Human donor cornea were obtained from Indiana Lion Eye Bank in 4 °C Optisol® GS medium. Corneal endothelium with Descemet's membrane was peeled off in Corneal Viewing Chamber (Stephens Instruments) using Submerged Cornea Using Backgrounds Away (SCUBA) technique. Peeled corneal endothelium sheet was processed immediately or stored in RNA*later*® (AM7020, Ambion) at 4 °C. Corneal endothelium sheet was rapidly frozen in liquid nitrogen and grinded followed by RNeasy column (Qiagen) purification.

Mouse corneal endothelium: Mouse cornea with sclera skirt was dissected from the globe. Corneal endothelium with Descemet's membrane was peeled off followed by RNA extraction similarly as described above.

FECD corneal endothelium: Patients diseased cornea endothelium samples were collected during Decrements Membrane Endothelial Keratoplasty (DMEK) surgery, and shipped on ice overnight in Optisol® GS medium. Corneal endothelium sheet was put into RNA*later*® in 4 °C till RNA extraction or processed immediately upon arrival. RNA extraction steps were the same as described above.

Immortalized HCEC cell line: HCEC cells were cultured in OptiMEM complete medium to confluent, RNA extraction steps were the same as described above.

### 2.3. PCR, qRT-PCR and Nested PCR

Complementary DNA was generated with High Capacity RNA-to-cDNA Kit (Applied Biosystems) at 10 ng RNA/μL reverse transcription. Sequences of human and mouse gene primers used are listed in Table S1 and Table S2, respectively. Conventional PCR was performed with MyCycler Thermal cycler (Bio-Rad) following the AmpliTaq® 360 DNA Polymerase protocol (Applied Biosystems). Real-time qPCR reactions were set up in triplicate using SYBR Green PCR Master Mix (Agilent Technologies). All assays used the same PCR conditions. A $2^{-\Delta\Delta Ct}$ experimental design was used for relative quantification and normalized to ACTB (mouse) or GAPDH (human) for differential expression levels of target genes. Nested PCR was conducted for genes with no CT value in real-time qPCR. An additional 40 cycles of PCR were conducted on reverse transcription PCR product using the same gene primers.

### 2.4. Immortalized HCEC Culture

Immortalized HCEC (Schmedt et al., 2012) were cultured at 37 °C, 5% $CO_2$ in appropriate plates or flasks coated with undiluted FNC Coating Mix® (AthenaES). Complete medium (OptiMEM-I®; Invitrogen) contains 8% FBS (Hyclone Laboratories Inc.), EGF 5 ng/mL (Millipore), pituitary extract 100 μg/mL (Hyclone Laboratories), calcium chloride 1.8 mM, 0.08% chondroitin sulfate (Sigma-Aldrich), gentamicin 50 μg/mL, and antibiotic/antimycotic solution diluted 1:100 (Invitrogen).

### 2.5. Immunofluorescence Staining

Excised mouse eyes or human donor cornea button were fixed in 4% paraformaldehyde in 0.1 mol/L phosphate buffer (pH 7.4) at 4 °C overnight and paraffin embedded. Five-micrometer sections were then mounted on Super Frost slides (Fisher Scientific). The sections were de-paraffinized and hydrated in a graded ethanol series (100%, 95% and 70% and 50% ethanol and $ddH_2O$ for 5 min each) and subject to antigen retrieval in 10 mM Na-citrate, then blocked with 2% BSA in PBS and incubated overnight at 4 °C with 1st antibodies. After washes in PBS, slides were incubated with Fluor-conjugated 2nd antibody for one hour and washed. Sections were mounted with prolong anti-fade mounting reagent with DAPI (Molecular Probes, Life Technologies) and imaged with AxioImager M1 microscope with AxioCam MRm camera (Zeiss).

The following antibodies were used: Rabbit polyclonal anti-Glutaminase (GLS1) antibody 1:200 (ab93434, Abcam); Rabbit anti-GLS2 antibody 1:200 (ab113509, Abcam); Mouse monoclonal anti-GGT1 antibody 1:200 (ab55138, Abcam); Rabbit anti-ZO1 1:200 (402200, Life Technologies); Mouse anti-ZO1 1:200 (339100, Invitrogen); Rabbit anti-Nitrotyrosine 1:200 (A-21285, Thermo Scientific); Secondary Alexa-488 and Alexa-568 antibodies (Molecular Probes) were used at 1:200 concentrations. Mean intensity (MFI) quantification of endothelium was conducted using ImageJ.

### 2.6. Hematoxylin and Eosin (H&E) Staining

Deparaffinized sections (5 μm) were stained with Hematoxylin and Eosin (H&E), and imaged with AxioImager M1 (Zeiss).

### 2.7. Alizarin Red Staining of Corneal Endothelium

As previously described (Park et al., 2012), rabbit and/or human cornea button was briefly immersed and rinsed with pH 4.2 0.9% saline, then stained with pH 4.2 0.2% Alizarin Red 0.9% saline for 2 min, and rinsed with pH 7.2 0.9% saline.

### 2.8. Ammonia Assay

HCEC seeded at $2 \times 10^5$/mL in 12-well plates were cultured to confluence, then incubated with DMEM (phenol red free, glucose free, glutamine-free, pyruvate-free, Gibco #A1443001) for 24 h with 10% dialyzed FBS, glucose 1 g/L, and glutamine at concentrations of 0.1, 0.5, 1, 2 and 4 mM. Medium supernatant after centrifugation was measured for ammonia concentration with a colorimetric assay kit (K370-100, Biovision).

### 2.9. Intracellular ATP Assay

HCEC seeded at $1.5 \times 10^4$/mL in 12-well plate were cultured to sub-confluent, then put under serum-free conditional DMEM medium (glucose free, glutamine-free, pyruvate-free, Gibco #A1443001) with glucose and/or glutamine supplementation for 12 h before measurement. ATP is extracted by a boiling water method (Yang et al., 2002), and measured by luciferin-luciferase based ATP assay kit (A22066, Molecular Probes).

### 2.10. Isotope Labeling, Metabolite Extraction and Measurement in HCEC

HCEC cells were cultured with either U-$^{13}C_5$-L-Glutamine or U-$^{13}C_6$-D-glucose for 12 h. Intracellular metabolite extraction was performed using a published protocol (Sellick et al., 2011). In brief, HCEC seeded at $5 \times 10^5$ cells/T75 flask in 8% FBS OptiMEM-I were grown to confluent for 4 days then switched to serum-free OptiMEM-I for 12 h. Then the cells were labeled with serum-free DMEM conditional medium with 4 mM U-$^{13}C_5$-L-Glutamine (CLM-1822-H, Cambridge Isotope Laboratories) and 13.9 mM (2.5 g/L) D-glucose, and incubated for 12 h. Serum-free DMEM conditional medium was made using DMEM (glucose free, glutamine-free, pyruvate-free, GIBCO® #A1443001) supplemented with calcium chloride 1.8 mM, 0.08% chondroitin sulfate (Sigma-Aldrich), and the corresponding isotope-labeled glucose and/or glutamine. An experiment with 2.5 g/L U-$^{13}C_6$-D-glucose (CLM-1396-0, Cambridge Isotope Laboratories) and 4 mM L-glutamine was also performed as verification. Labeled cells were washed three times with ice-cold 0.9% NaCl, and quenched with 2 mL ice cold 100% methanol. Cells were scraped off the T75 flask pellet and removed together with 2 mL methanol into centrifuge tube, vortexed thoroughly, centrifuged at 8000 *g* for 2 min. Supernatants were collected and the cell pellet was resuspended with 900 μL of 90% methanol, vortexed thoroughly, centrifuged and supernatant collected. The procedure was repeated for a second time with 750 μL of 90% methanol. Total supernatant of two tubes (1500 μL each) was kept stationary at −20 °C for 1 h, then centrifuged at 15,000 *g* for 5 min at 4 °C and the supernatant (1000 μL each) was collected to two new tubes. Then the sample was dried in a centrifugal evaporator at room temperature about 1 h, then the supernatant in the two tubes was pooled together and dried overnight.

The abundance of each isotopologue was detected using GC–MS. The fraction of each isotopologue and the contribution of $^{13}C$ to the total carbon pool of each metabolite were calculated as previously reported (Nanchen et al., 2007). In brief, the isotopologue distributions were corrected based on the natural abundance of elements, and the fraction is the contribution of each isotopologue to the total abundance of all the isotopologues. The contribution of $^{13}C$ to the total carbon pool of each metabolite is the weighted average of all the labeled isotopologues according to the fraction distribution.

### 2.11. Fresh Rabbit Corneal Perfusion

Rabbit cornea perfusion followed the protocol as described previously (Li et al., 2016). Ringer's solutions contain (mM): 153.5 $Na^+$, 4 $K^+$, 1.4 $Ca^{2+}$, 0.6 $Mg^{2+}$, 113.2 $Cl^-$, 1 $HPO_4^{2-}$, 16.4 gluconate$^-$ and 28.5 $HCO_3^-$. All solutions were equilibrated with 5% $CO_2$, pH adjusted to 7.5 and osmolarity adjusted to 295 mOsm/L with sucrose. 5 mM glucose and/or 1 mM glutamine were added. BR Glc/— contains 5 mM glucose, while BR Glc/Gln contains 5 mM glucose and 1 mM glutamine. Perfusion solutions were maintained at 37 °C in a water bath during experiment.

### 2.12. Alternate Corneal De-Swelling Experiments

Four different Ringer's solutions were used: 1) BR Base; 2) BR Glc/Gln; 3) BR Glc/— and 4) BR —/Gln. BR Base contains (mM): 148.5 $Na^+$, 4 $K^+$, 1.4 $Ca^{2+}$, 0.6 $Mg^{2+}$, 103.2 $Cl^-$, 28.5 $HCO_3^-$. The addition of 5 mM glucose and/or 2 mM glutamine was made to BR base to get BR Glc/Gln, BR Glc/—, and BR —/Gln. All solutions were adjusted to pH 7.5 with 1 N HCl and osmolarity 295 mOsm/L with mannitol.

For rabbit cornea: rabbit eye balls stored on ice were shipped overnight from a regional supplier (Pel-Freez Biologicals). Corneal thickness was measured immediately before dissecting as data point of time zero by Optical Coherence Tomography (OCT) with anterior segment attachment (OptoVue iVue SD-OCT). Then eye balls were assigned to experimental groups 1) Glc/Gln 2) Glc/— and 3) —/Gln and dissected to cornea button with sclera skirt, rinsed and mounted with corresponding Ringer's solution. Cornea with sclera skirt was mounted onto a Barron® artificial anterior chamber (K20-2125, Katena Products, Inc.) and anterior chamber was filled with 350 μL Ringer's solution corresponding to the assigned group. Corneal thickness was measured every 15 min. Artificial tears (Refresh®) were applied on the epithelial surface every 15 min after OCT measurement, and Barron Chamber with mounted cornea is put in 37 °C incubator when not being measured. The corneal thickness was measured for 150 min. After the experiment, Ringer solution (~350 μL) is collected and prepared for GC–MS analysis for residual glutamine and glucose. Then cornea button was stained with Alizarin Red for corneal endothelium visualization and cell density was counted under light microscope (Park et al., 2012).

For human donor cornea: De-identified human donor cornea with sclera skirt was obtained from the Indiana Lions Eye Bank, stored in 4 °C Optisol® GS medium until experiments. Cornea with sclera skirt was rinsed with ice-cold BR base solution, then soaked in ice-cold BR base solution for 1 h to let it swell. Then the human cornea was mounted as for rabbit cornea with 300 μL BR Glc/Gln or BR Glc/—, and monitored for central corneal thickness with OCT every 15 min for 165 min. Artificial tears (Refresh®) were applied after each measurement, and Barron® Chamber with mounted cornea was put in 37 °C incubator between measurement. After the experiment, Ringer (~300 μL) is collected and prepared for GC–MS analysis for residual glutamine and glucose. Then cornea button was stained with Alizarin Red for corneal endothelium visualization and cell density was counted under light microscope (Park et al., 2012).

### 2.13. Metabolite ex vivo Consumption Rate Estimation

The Ringer solutions in the Barron® chamber after the ex vivo deswelling experiment were collected and prepared for GC–MS analysis of residual glutamine and/or glucose. In brief, the Ringer's solution in the artificial anterior chamber was collected with a 1 mL syringe through the connecting tubing of the chamber. A 10 μL sample was mixed with 5 μL of 5 mM U-$^{13}C_6$-glucose and 5 μL of 2 mM U-$^{13}C_5$-glutamine (which serve as internal standards), and 500 μL of 90% methanol. The sample was kept stationary at −20 °C for 1 h, then centrifuged at 15,000 *g* for 5 min at 4 °C. The supernatant (500 μL) was collected to a new tube and dried in a centrifugal evaporator at room temperature overnight. The levels of residual glucose and glutamine were measured using gas chromatography–mass spectrometry (GC–MS) as reported previously (Tennessen et al., 2014). Quantification was achieved using the $^{13}C$–labeled internal standards. Fresh Ringer's solutions (BR Glc/Gln, BR Glc/— and BR —/Gln) were measured in parallel as control.

Total glucose or glutamine consumption per cornea was calculated by subtracting residual glucose and/or glutamine measured after the de-swelling experiment from glucose and/or glutamine concentration measured in fresh Ringer's solution. Consumption per corneal endothelial cell was calculated by dividing the total consumption with total cornea endothelial count of each cornea. Total number of corneal endothelial cells per cornea was calculated as the product of corneal endothelial density measured from Alizarin Red visualization and cornea dome surface area. The glucose and/or glutamine consumption rates per cell per hour were further calculated by dividing consumption per cell by time elapsed in each experiment.

For surface area calculation, rabbit cornea diameter 13.2 mm and radius of curvature 7.26 mm were used (Bozkir et al., 1997), and human cornea diameter 11.5 mm and radius of curvature 7.75 mm were used (Ganguli et al., 1975). Rabbit and human corneal endothelium density and total cell count are shown in Table S3.

Equation used for surface area calculation was

$$A = 2\pi r\left(r - \sqrt{r^2 - (a/2)^2}\right)$$

in which $A$ is the surface area of a corneal endothelium sheet formed partial sphere, $r$ is the radius of curvature, and $a$ is the cornea diameter.

### 2.14. Statistical Analysis

Statistical analysis was performed using SPSS Statistics v21 (IBM Corporation) and GraphPad Prime 6.0c (GraphPad Software, Inc.). Student *t*-test was used for two-group comparison. One-way ANOVA with post-hoc Tukey was used for data with more than two groups.

## 3. Results

### 3.1. Corneal Endothelium Expresses Glutamine Metabolic Enzymes and Glutamine Transporters

The $NH_3$:$2H^+$ cotransporter SLC4A11 (Zhang et al., 2015) is highly expressed in CE (Chng et al., 2013). This discovery led us to hypothesize that CE processes ammonia and is likely to metabolize glutamine. Therefore, we examined if glutaminolysis enzymes and glutamine/glutamate transporters are expressed in human and mouse CE. Consistent with our hypothesis, both human and mouse CE express mRNAs that encode phosphate-activated glutaminase type 1 (GLS1, kidney-type) and type 2 (GLS2, liver-type) (Fig. 1A). In addition, we observed a similar expression profile for gamma-glutamyl-transpeptidase (GGT), which has membrane glutaminase activity (Fig. 1A) and functions together with membrane glutamate excitatory amino acid transporters (EAATs) (Zhang et al., 2005). The expression of GLS1, GLS2 and GGT in human CE tissue was verified by immunostaining of healthy human donor cornea sections (Fig. 1B). Consistent with these observations, we also determined that immortalized human corneal endothelium cell line (HCEC) also expressed GLS1, GLS2, and GGT (Fig. 1C, D). Furthermore (Fig. 1D), GLS1 immunostaining shows a punctate perinuclear staining pattern consistent with mitochondrial localization of GLS1 reported in other tissues (Kvamme et al., 2000), and GGT immunostaining exhibits a pericellular staining indicating plasma membrane localization as reported in other cell types (West and Hanigan, 2010).

In addition to our analysis of metabolic enzymes, we also screened eleven putative glutamine transporters for expression in HCEC (Fig. 1C). Our analysis revealed that HCECs express 10 of these transporters, including the $Na^+$-glutamine/neutral amino acid antiporter (SLC1A5), $Na^+$-glutamine co-transporter (SLC6A19). Furthermore (Fig. 1D), GLS1 immunostaining shows a punctate perinuclear staining pattern consistent with mitochondrial localization of GLS1 reported in other tissues (Kvamme et al., 2000), and GGT immunostaining exhibits surface staining indicating plasma membrane localization as reported in other cell types (West and Hanigan, 2010) (SLC38A1, SLC38A2), glutamine/large neutral amino acids antiporter (SLC7A5), glutamine/small neutral amino acids antiporter (SLC7A8), $Na^+$-glutamine/$H^+$ antiporter (SLC38A3, SLC38A5, SLC38A7) and $Na^+$-neutral amino acid transporter (SLC38A8). For glutamate transport (EAATs), both human CE tissue (Fig. 1A) and HCEC (Fig. 1C) express EAAT1, EAAT2 and EAAT3. Overall, these results demonstrate that CE metabolism is capable of utilizing glutamine as energy source.

### 3.2. Glutamine is a Major Source of TCA Cycle Intermediate Pool in Corneal Endothelium

Given the high expression of enzymes and transporters involved in glutamine metabolism, we propose that CE utilizes aqueous humor glutamine via active uptake through glutamine transporters as well as conversion of glutamine to glutamate by GGT/EAATs complex. Glutamine and glutamate could then be actively metabolized in mitochondria into the TCA cycle to support energy production (Fig. 2A). To test our hypothesis, we first examined glutamine-derived ammonia release in HCEC. As expected, we observed a dose-dependent increase of ammonia production as glutamine concentration increases (Fig. 2B), suggesting that corneal endothelium can utilize glutamine efficiently. To further investigate if the glutamine is metabolized by GLS1/GLS2 in mitochondria, HCEC cells were fed 4 mM U-$^{13}C_5$-glutamine in the presence of 13.9 mM (2.5 g/L) glucose, and gas chromatography mass spectrometry (GC/MS) was used to measure $^{13}C$ incorporation into TCA cycle intermediates. Fig. 2C (schematic diagram), shows U-$^{13}C_5$-glutamine (m + 5 isotopologue, all 5 carbons are $^{13}C$) metabolism in mitochondria. First, conversion to glutamate and then to $^{13}C_5$-α-ketoglutarate (m + 5 isotopologue). The unlabeled fraction of α-ketoglutarate (m + 0, all 5 carbons are $^{12}C$) originates from unlabeled glucose or other unlabeled sources. Further oxidation of $^{13}C_5$-α-ketoglutarate (m + 5) in the TCA cycle produces $^{13}C_4$-fumarate (m + 4), $^{13}C_4$-malate (m + 4) and $^{13}C_4$-citrate (m + 4) labeling. The $^{13}C_4$-citrate (m + 4) is synthesized from $^{13}C_4$-oxaloactetae (derived from labeled glutamine in the first turn) and acetyl-coA (derived from unlabeled glucose). The m + 3 α-ketoglutarate isotopologue peak observed is the product from $^{13}C_4$-citrate, indicating $^{13}C_5$-glutamine originated carbon chain stays in the TCA cycle for a second turn. The sum of all labeled intermediates is ~50% of each intermediate indicating that glutamine contributes ~50% of the TCA cycle intermediate pool (Fig. 2C). The results were verified with glucose labeling (Fig. S1A), in which HCEC were fed with 13.9 mM U-$^{13}C_6$-glucose in the presence of 4 mM glutamine. Further experiments verified that 5.6 mM (1 g/L) and 13.9 mM (2.5 g/L) U-$^{13}C_6$-glucose did not change the percentage distribution of the labeled TCA cycle intermediates (Fig. S1B), suggesting that HCECs prefer metabolizing glutamine via the TCA cycle even in the presence of excess glucose.

### 3.3. Glutamine Supplies ATP for Corneal Endothelium Pump Function

Given the physiological function of the CE, we hypothesize that glutamine-derived ATP is required to supply energy for CE fluid transport. To test this hypothesis, we first measured intracellular ATP content in HCEC with conditional DMEM medium: 1) Glc/Gln: 27.8 mM (5 g/L) glucose +4 mM glutamine; 2) −/Gln: 4 mM glutamine; 3) Glc/−: 27.8 mM (5 g/L) glucose; 4) −/−: neither glucose nor glutamine. While ATP content was the highest in Glc/Gln medium and only slightly lower in −/Gln, ATP production was severely impaired in Glc/− and −/− conditions (Fig. 3A). These results indicate that glucose can only sustain half of the CE energy supply and are consistent with GC–MS data that only half of the TCA intermediates were derived from glucose (Fig. S1A).

In order to determine if the CE exhibits a similar reliance on glutamine metabolism in vivo, we examined the effect of glutamine supplementation on perfused freshly dissected ex vivo rabbit corneas. If

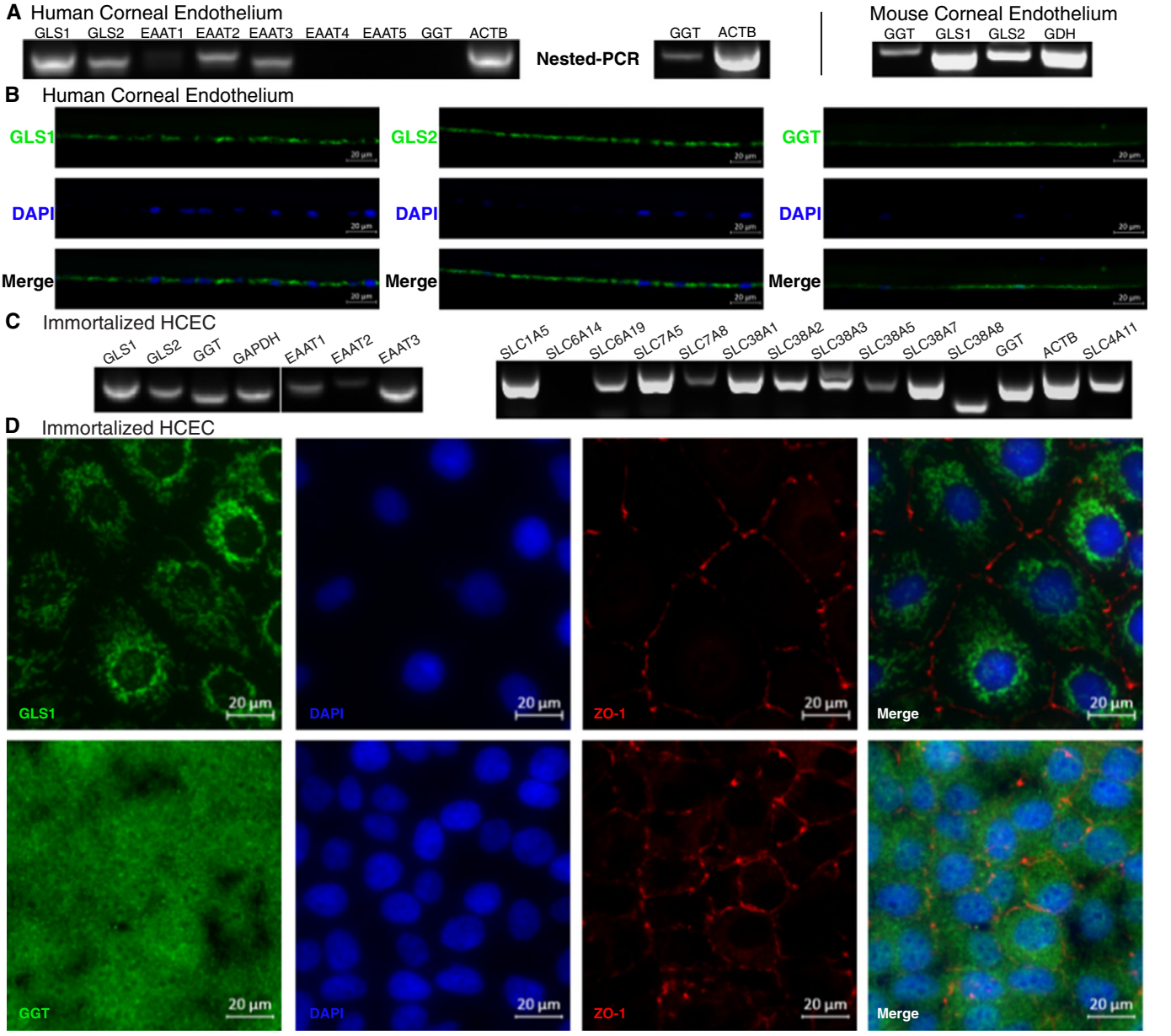


**Fig. 1.** Expression of glutaminase, glutamate transporters and glutamine transporters in corneal endothelium. (A) RT-PCR of human and mouse corneal endothelial tissue for glutaminase (GLS1, GLS2, GGT), glutamate dehydrogenase (GDH) and glutamate transporters (EAAT1-5); ACTB: beta actin. (B) Immunofluorescence staining of human cornea section showing GLS1, GLS2 and GGT expression in cornea endothelium; (C) RT-PCR of HCEC showing expression of GLS1, GLS2, GGT, EAAT1-3, ten glutamine transporters as well as SLC4A11. Glutamine transporters expressed: SLC1A5, $Na^+$-glutamine/neutral amino acid antiport; SLC6A19, $Na^+$-glutamine co-transport; SLC7A5, glutamine/large neutral amino acid antiport; SLC7A8, glutamine/small neutral amino acid antiport; SLC38A1, $Na^+$-glutamine cotransport; SLC38A2, $Na^+$-glutamine cotransport; SLC38A3, $Na^+$-glutamine/$H^+$ antiport; SLC38A5, $Na^+$-glutamine/$H^+$ antiport; SLC38A7, $Na^+$-glutamine/$H^+$ antiport; SLC38A8, $Na^+$-Neutral Amino Acid Transporter. GAPDH: glyceraldehyde 3-phosphate dehydrogenase. (D) Immunofluorescence staining of GLS1 (upper) and GGT (lower) in HCEC.

glutamine is beneficial for energy production, the corneal thickness will be better maintained (i.e., thinner) over a prolonged perfusion period as a result of better pump activity. Indeed, central corneal thickness (CCT) was 2.5 μm less in glutamine supplemented corneas after 3.5 h perfusion (Fig. 3B). We then estimated the rate of glutamine consumption by corneal endothelium in vivo by performing a modified version of the classic corneal de-swelling experiment with ex vivo 4 °C stored rabbit and human corneas (Maurice, 1972). Briefly, the Ringer's solution with glucose and/or glutamine supplementation filled an artificial anterior chamber in contact with the CE apical surface (Fig. S2A). The cold cornea is swollen because the endothelial pump is inactive. When warmed up to 37 °C, the cornea will deswell due to re-activation of metabolism and in turn ion and fluid transport activity. The deswelling rate is a measure of CE pump efficiency. If glutamine metabolism enhances energy production, one would expect a faster de-swelling rate with glutamine addition. Indeed, in both rabbit and human cornea, glutamine supplementation facilitated a faster deswelling rate (Fig. 3C, E). At the end of the experiments, the Ringer's solution was collected and residual glucose and glutamine was measured by GC–MS. The glucose and/or glutamine consumption rate per cell was estimated from the total consumed glutamine/glucose and total corneal endothelial cell count determined from Alizarin Red staining (Fig. S2B). For rabbit CE, 0.48 ± 0.06–0.71 ± 0.08 pmol/cell/h glucose and 0.33 ± 0.01–0.60 ± 0.02 pmol/cell/h glutamine was consumed (Fig. 3D). For human CE, 0.77 ± 0.01–0.82 ± 0.06 pmol/cell/h glucose and 0.39 ± 0.04 pmol/cell/h glutamine was consumed (Fig. 3F). There is a close consistency between rabbit and human CE here, as well as to previous report of glucose consumption 0.2 pmol/cell/h (7.4 μg/$cm^2$/h, 2000 cell/$mm^2$ density assumed) in

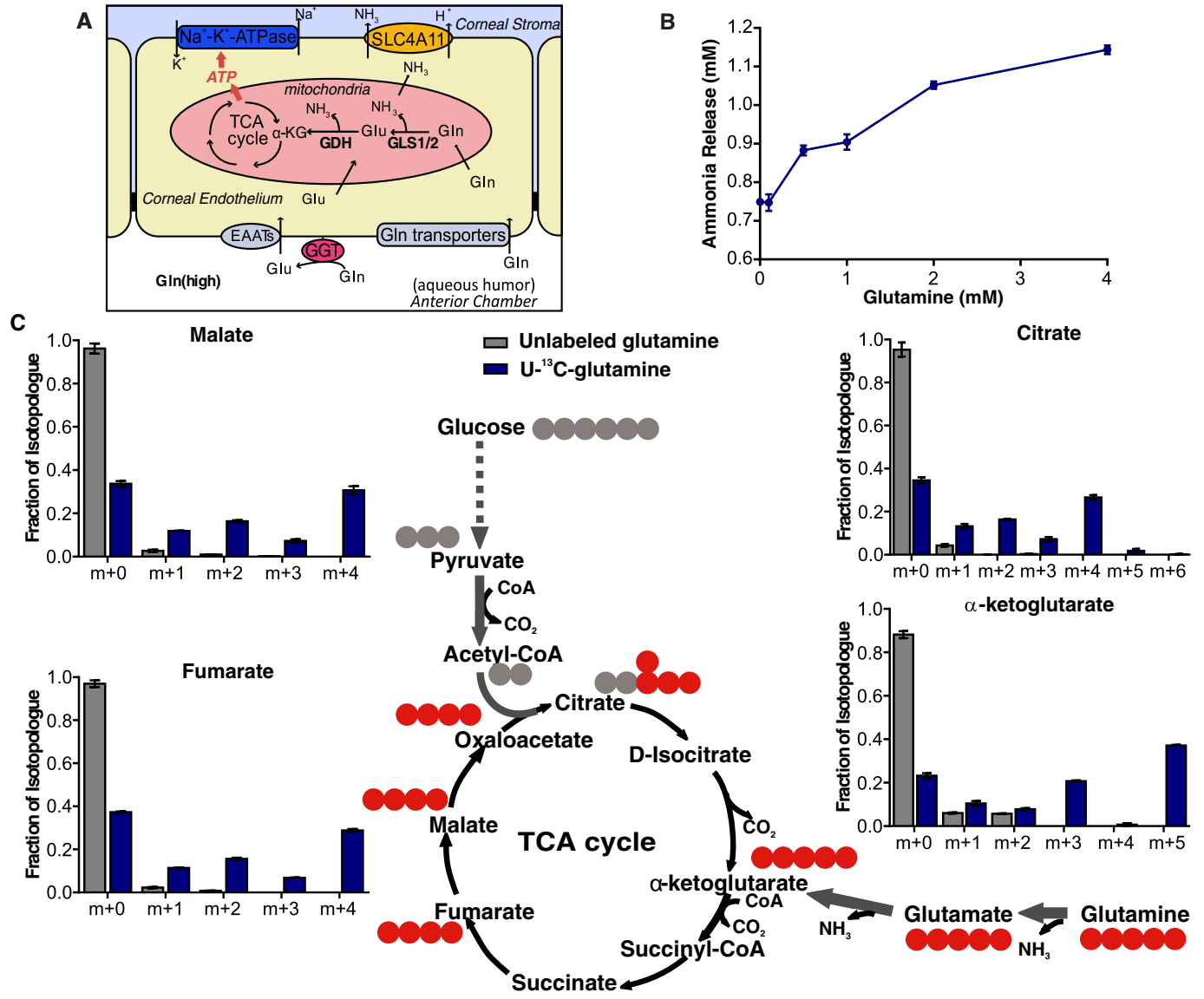


**Fig. 2.** Glutamine contributes to the TCA cycle in HCEC. (A) Schematic illustration of proposed glutamine metabolism in corneal endothelium; (B) Ammonia release is dependent on glutamine concentration in HCEC; (C) GC–MS results show ~50% of carbons in the TCA intermediates are from glutamine. $^{13}C$ is illustrated as red dot, whereas $^{12}C$ is gray dot. Cells were cultured for 12 h in 4 mM U-$^{13}C_5$-glutamine and 13.9 mM unlabeled glucose in experimental group (blue bars), whereas 4 mM unlabeled glutamine and 13.9 mM unlabeled glucose in control (gray bars). The isotopologue distributions were corrected based on the natural abundance of elements (gray bars), and the labeled fraction (blue bar) is the contribution of each isotopologue to the total abundance of all the isotopologues.

cultured rabbit CE (Zurawski et al., 1989). Taken together, these data show that glutamine enhances endothelial pump function by sustaining ATP production in both rabbit and human CE.

### 3.4. Loss of SLC4A11 Ammonia Transporter Impairs Glutaminolysis in Corneal Endothelium

We hypothesize that the SLC4A11 ammonia transporter is needed to remove the ammonia produced from active glutaminolysis. To test this hypothesis, we looked for signs of potential ammonia toxicity and alterations in glutaminolysis enzyme expression in the *Slc4a11*$^{-/-}$ mouse corneal endothelium. The *Slc4a11*$^{-/-}$ C57BL/6 mice (Han et al., 2013) recapitulates the human CHED phenotype (Kirkness et al., 1987) showing diffuse corneal edema (Fig. 4A), vacuolated CE, and thickened Descemet's (basement) membrane (Fig. 4B). Consistent with the role of Slc4a11 in ammonia transport, we observed that *Slc4a11*$^{-/-}$ mouse CE exhibits elevated levels of nitrotyrosine staining, which is commonly used as a general marker of ammonia toxicity (Montoliu et al., 2011) (Fig. 4C, D). qRT-PCR analysis also revealed that glutaminolysis was disrupted in these mutant mice, as *Gls1* expression is up-regulated by 3-fold whereas *Gls2* expression is diminished in *Slc4a11*$^{-/-}$ CE at an early age of 12 weeks (Fig. 4E). Furthermore, nested-PCR revealed no *Gls2* and *Ggt* expression could be detected in *Slc4a11*$^{-/-}$ CE (Fig. 4F). The Gls1 and Gls2 expression changes were further confirmed by immunofluorescence at 40 weeks of age (Fig. 4G).

Since *SLC4A11* expression is down-regulated in Fuchs' Endothelial Corneal Dystrophy (FECD) post-surgical CE samples (Gottsch et al., 2003), we next examined the expression of *GLS1*, *GLS2* and *SLC4A11* in post-surgical CE specimens from FECD patients via qRT-PCR. We observed a similar trend of *GLS1* upregulation and *GLS2* downregulation associated with underexpressed *SLC4A11* in human FECD as was seen in the *Slc4a11*$^{-/-}$ CHED mouse model (Fig. S3). While *SLC4A11* and *GLS1* changes did not show statistical significance possibly due to the diverse genetic background of FECD patients, GLS2 expression was significantly decreased. Overall, these results demonstrate that SLC4A11 is required for normal glutaminolysis in the CE.

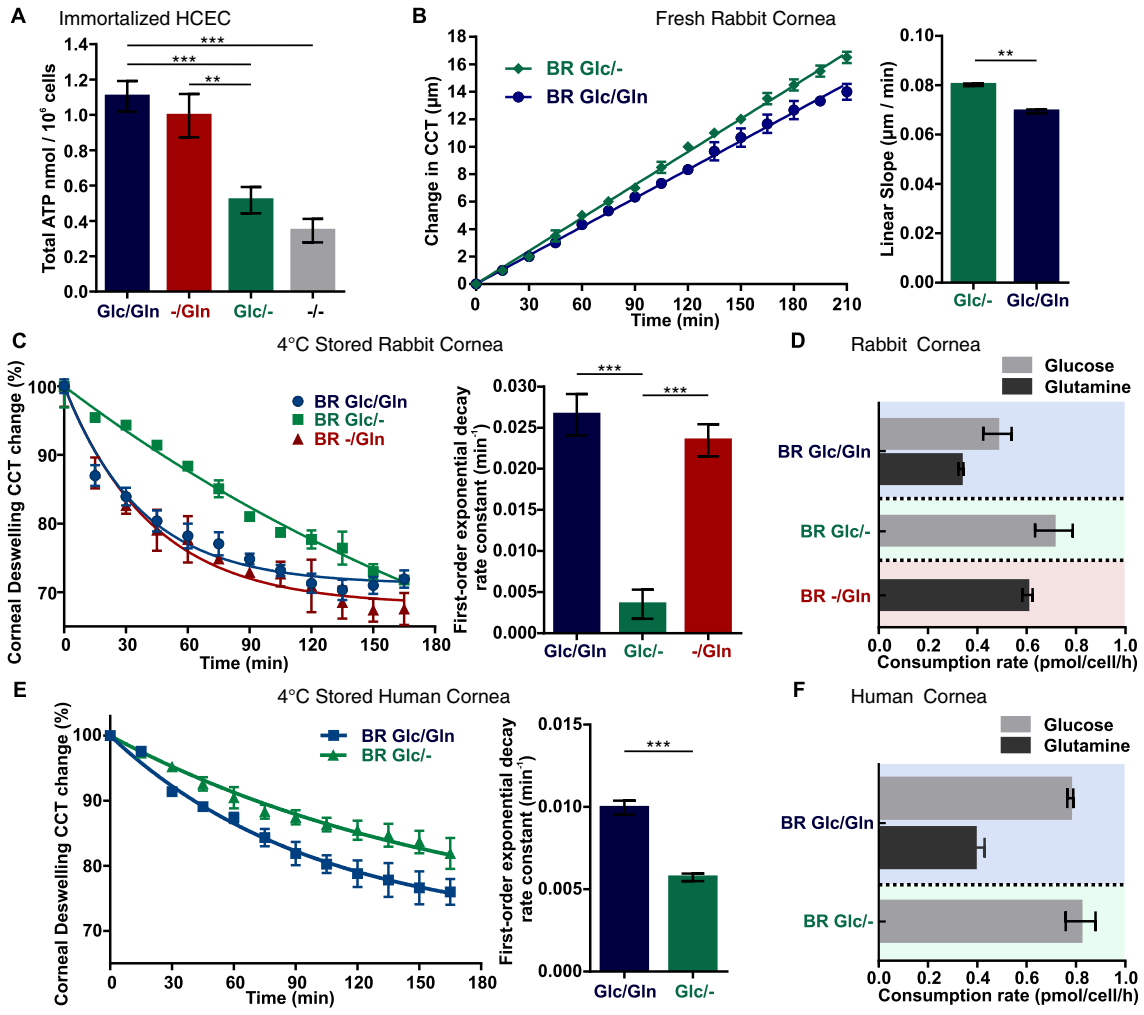


**Fig. 3.** Glutamine supplies energy for corneal endothelial pump function. (A) ATP levels in cultured HCEC in conditional media (n = 23 in each); (B) Central corneal thickness (CCT) is better maintained with glutamine-supplemented perfusion. Left: time course of CCT change. Right: linear slope comparison. (C) Corneal deswelling curves in various Ringers from cold stored corneas: bicarbonate rich Ringer with glucose and glutamine (BR Glc/Gln); bicarbonate rich Ringer with glucose (BR Glc/−); and bicarbonate rich Ringer with glutamine (BR −/Gln). Left: time course of CCT changes. Right: first-order exponential decay rate constant comparison between groups. (D) Rabbit corneal endothelium glucose and glutamine consumption rate. (E) Cold stored human cornea deswelling curves in various Ringers: BR Glc/Gln and BR Glc/−. Left: time course of CCT changes. Right: first-order exponential decay rate constant comparison between groups. (F) Human corneal endothelium glucose and glutamine consumption rate. Data are shown as mean ± s.e.m., $^{**}p < 0.01$; $^{***}p < 0.001$.

## 4. Discussion

Here we report that glutaminolysis is a significant contributor to energy production in support of CE pump function. Before this work, glucose was the only energy source known for CE pump (Laing et al., 1992; Zurawski et al., 1989). Our results demonstrate that glutamine is incorporated into TCA cycle intermediates, which augments ATP production, and accelerates the physiological pump function of CE. Loss of the $NH_3$:$H^+$ transporter disrupts expression of glutaminolysis enzymes and produces a potential ammonia toxicity phenotype.

Glutamine is the most abundant free amino acid in plasma (Curthoys and Watford, 1995). Mitochondrial glutamine metabolism was initially studied in renal, skeletal muscular, intestinal and brain physiology as a major player in nitrogen metabolism (Kovacevic and McGivan, 1983). For example, kidney proximal tubular epithelium upregulates glutaminolysis to extrude more $NH_4^+$ as acid equivalent under pathological chronic metabolic acidosis (Alleyne et al., 1982). Recently, more research has focused on the increased glutaminolysis activity in cancer cells after metabolic reprogramming, as glutaminolysis provides an additional source of biosynthetic precursors as well as energy for rapidly dividing cancer cells (Jin et al., 2016). Glutaminolysis has also been implicated in directing the differentiation of stem cells in neuronal and hematopoietic tissue (Agostini et al., 2016; Oburoglu et al., 2014). Here we report that glutaminolysis mainly sustains ATP production supporting fluid transport in terminally-differentiated non-proliferating corneal endothelium under physiological conditions. The generation of ATP from glutaminolysis can also support other ATP consuming cellular processes in CE, such as protein synthesis and RNA synthesis.

The capacity of a cell utilizing glutaminolysis not only provides the cell with an additional energy source on top of glucose, the utilization of glutaminolysis is as energy efficient as glucose oxidation, if not more. Complete oxidation of one glucose produces 36 ATP. Theoretically, glutaminolysis generates a total of 12 ATP in one turn of the TCA cycle with one carbon consumed, and the rest of the carbon chain stays in the TCA cycle for further ATP generation. (Glutamine enters the TCA cycle via α-ketoglutarate, and will generate 1 ATP by direct phosphorylation of GDP, 2 ATPs from $FADH_2$ generated during succinate → fumarate reaction, 9 ATPs from three NADHs generated from the α-ketoglutarate dehydrogenase, malate dehydrogenase and malate decarboxylase reactions.) One estimation shows that glutaminolysis can generate up to 17.5 mol ATP per mol of glutamine consumed (Le et al., 2012).

The presence of glutamine accelerated the CE pump function, indicating the involvement of glutamine metabolism. Our estimates of this involvement however, rely on cultured cells using supraphysiological

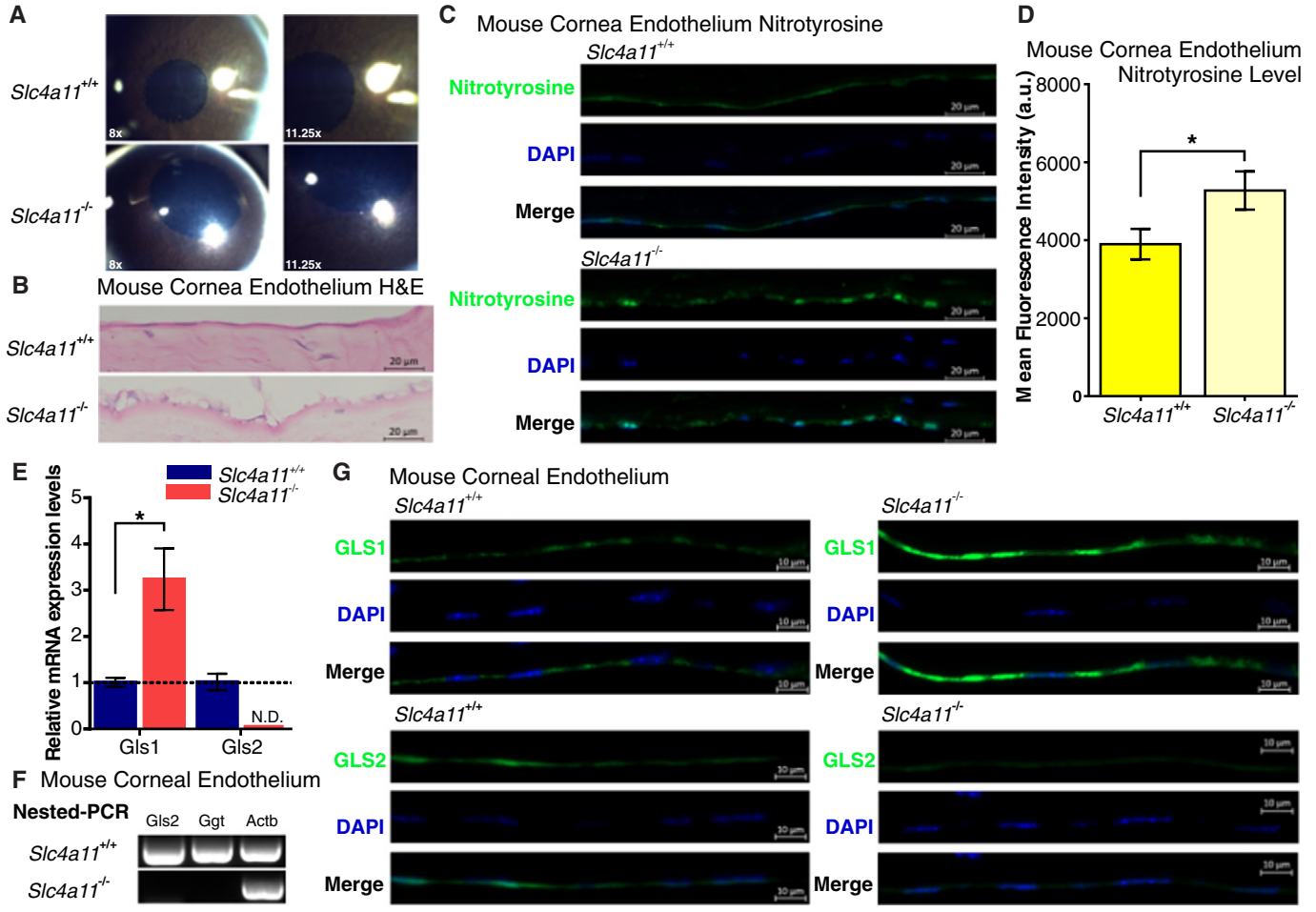


**Fig. 4.** *Slc4a11*$^{-/-}$ mouse corneal endothelium shows signs of ammonia toxicity and altered glutaminolysis enzymes. (A) Photography of *Slc4a11*$^{+/+}$ and *Slc4a11*$^{-/-}$ mouse cornea, shows diffuse edema (increase of light reflection in clear stroma) in 12-week *Slc4a11*$^{-/-}$. (B) H&E staining of 40-week *Slc4a11*$^{+/+}$ and *Slc4a11*$^{-/-}$ mouse cornea section shows endothelial vacuolation and Descemet's (basement) membrane thickening. (C) Nitrotyrosine immunostaining shows increased intensity in 40-week old *Slc4a11*$^{-/-}$ corneal endothelium, suggesting ammonia toxicity. (D) Quantification of nitrotyrosine staining by mean fluorescence intensity. Quantification of the mean fluorescence intensity was achieved by selecting corneal endothelium layer as region of interest (n = 3 in each group). (E) Real-time qPCR of 12-week *Slc4a11*$^{+/+}$ and *Slc4a11*$^{-/-}$ mouse cornea endothelium shows upregulated Gls1 and non-detectable (N.D.) Gls2 in *Slc4a11*$^{-/-}$. (F) Nested-PCR verification of Gls2 and Ggt are not detectable in 12-week *Slc4a11*$^{-/-}$ cornea endothelium. (G) Immunostaining verification of Gls1 and Gls2 expression changes in 40-week *Slc4a11*$^{+/+}$ and *Slc4a11*$^{-/-}$ mouse cornea endothelium are consistent with real-time qPCR results of 12-week mouse. Data are presented as mean ± s.e.m., $^{*}p < 0.05$.

culture conditions, e.g. 4 mM glutamine versus the ~0.5 mM aqueous humor glutamine concentration. Since the GC–MS data (Fig. 2 and Supplemental Fig. 1) for estimating the percentage contribution of glutamine and glucose into TCA cycle intermediates was obtained under these conditions, the exact carbon contribution from these two energy sources into the TCA cycle under physiological conditions will require further investigation.

Currently in clinical practice, glutamine is not included in irrigation solutions for ophthalmic surgeries. As such, our findings suggest that glutamine supplementation for corneal endothelium protection and functional support could be used clinically during and after ophthalmic procedures. Glutamine supplementation may provide a way to increase and possibly more quickly reactivate CE pump function after cataract surgery and corneal transplant.

Here we also report that glutaminolysis is significantly impaired in CE lacking the ammonia transporter SLC4A11, shedding some light on the pathophysiological mechanisms that lead to the developmental and/or degenerative diseases caused by *SLC4A11* mutations. These disorders include CHED: congenital developmental corneal endothelial disease (Vithana et al., 2006); Harboyan Syndrome: degenerative progressive sensorineural deafness with CHED (Siddiqui et al., 2014); Peters anomaly: developmental deficit of anterior segment of the eye (Weh et al., 2014); and FECD: age-related degenerative corneal endothelial disease (Vithana et al., 2008). In fact, SLC4A11 is widely expressed in cornea, kidney, inner ear, salivary glands, thyroid, mammary gland, testis, trachea, esophagus, pancreas, liver, spleen, and cerebellum (Damkier et al., 2007; Lopez et al., 2009; Park et al., 2004; Parker et al., 2001), suggesting that this relationship between SLC4A11 and glutaminolysis may be ubiquitous.

Interestingly, a recent report shows that SLC4A11 knock-down abolishes p53-ser15 phosphorylation in response to physiological high osmolality experienced by bovine nucleus pulposus intervertebral disc cells (Mavrogonatou et al., 2015). This is consistent with our observation of *GLS2* downregulation (Fig. 4C), because p53 is an enhancer of *GLS2* gene expression by direct binding to the response element BS2 (Suzuki et al., 2010). More interestingly, *SLC4A11* was also shown to be a target gene of p53, which is upregulated in response to DNA damage in mouse and human fibroblasts (Younger et al., 2015). Taken together, these reports and our observations here, indicate that the regulation of SLC4A11 and glutaminolysis goes hand in hand with major metabolic regulators, such as p53, in a variety of cell types.

## Funding Sources

The research is financially supported by NIH grant 5R01EY008834 (JAB); 5P30EY019008 (Vision Science Core Grant); 5R00GM101341-05

and 1R35GM119557-01 (JMT); Grant-in-Aid of Research from the National Academy of Sciences, administered by Sigma Xi Scientific Society (WZ); Eye Bank Association of America Richard Lindstrom Research Grants (WZ); American Optometric Foundation William C. Ezell Fellowship (WZ).

## Conflict of Interests

None to declare.

## Author Contributions

W.Z., H.L., and J.A.B. conceived the experiments, W.Z., H.L., J.M.T., and J.A.B. wrote the manuscript, W.Z., H.L., F.W.P., J.M.T. and J.A.B. edited the manuscript. W.Z., H.L., D.O. and S.L. performed the experiments. W.Z. J.M.T. and J.A.B. secured funding. M.F. and F.W.P. provided clinical samples. M.F., F.W.P., and J.M.T. provided expertise and feedback.

## Acknowledgments

We genuinely thank Mr. Mark Soper from the Indiana Lions Eye Bank and Dr. Marianne Price from the Cornea Research Foundation of America for facilitating the acquisition of human corneas. We thank Dr. Ula V. Jurkunas from the Massachusetts Eye & Ear Infirmary for the gift of immortalized HCEC, and Dr. Eranga N. Vithana from the Singapore Eye Research Institute for providing the *Slc4a11*$^{-/-}$ mouse. We thank Dr. Yijun Zhang and Edward Kim for their technical support with experimental procedures.

## Appendix A. Supplementary data

Supplementary data to this article can be found online at http://dx.doi.org/10.1016/j.ebiom.2017.01.004.

## References

Agostini, M., Romeo, F., Inoue, S., Niklison-Chirou, M.V., Elia, A.J., Dinsdale, D., Morone, N., Knight, R.A., Mak, T.W., Melino, G., 2016. Metabolic reprogramming during neuronal differentiation. Cell Death Differ. 23, 1502–1514.

Alleyne, G.A., Lupianez, J.A., McFarlane-Anderson, N., Hortelano, P., Benjamin, J., Barnswell, J., Scott, B., 1982. Glutamine metabolism in metabolic acidosis. CIBA Found. Symp. 87, 101–119.

Barfort, P., Maurice, D., 1974. Electrical potential and fluid transport across the corneal endothelium. Exp. Eye Res. 19, 11–19.

Bonanno, J.A., 2012. Molecular mechanisms underlying the corneal endothelial pump. Exp. Eye Res. 95, 2–7.

Boonstra, F., Claerhout, I., Hol, F., Smit, G., van Collenburg, J., Meire, F., 2002. Corneal decompensation in a boy with Kearns-Sayre syndrome. Ophthalmic Genet. 23, 247–251.

Bourne, W.M., 2003. Biology of the corneal endothelium in health and disease. Eye (Lond.) 17, 912–918.

Bozkir, G., Bozkir, M., Dogan, H., Aycan, K., Guler, B., 1997. Measurements of axial length and radius of corneal curvature in the rabbit eye. Acta Med. Okayama 51, 9–11.

Chang, T.S., Johns, D.R., Stark, W.J., Drachman, D.B., Green, W.R., 1994. Corneal decompensation in mitochondrial ophthalmoplegia plus (Kearns-Sayre) syndrome. A clinicopathologic case report. Cornea 13, 269–273.

Chng, Z., Peh, G.S., Herath, W.B., Cheng, T.Y., Ang, H.P., Toh, K.P., Robson, P., Mehta, J.S., Colman, A., 2013. High throughput gene expression analysis identifies reliable expression markers of human corneal endothelial cells. PLoS One 8, e67546.

Curthoys, N.P., Watford, M., 1995. Regulation of glutaminase activity and glutamine metabolism. Annu. Rev. Nutr. 15, 133–159.

Damkier, H.H., Nielsen, S., Praetorius, J., 2007. Molecular expression of SLC4-derived Na+-dependent anion transporters in selected human tissues. Am. J. Physiol. Regul. Integr. Comp. Physiol. 293, R2136–R2146.

Dorrepaal, S.J., Cao, K.Y., Slomovic, A.R., 2007. Indications for penetrating keratoplasty in a tertiary referral centre in Canada, 1996–2004. Can. J. Ophthalmol. 42, 244–250.

Ganguli, D., Roy, I.S., Biswas, S.K., Sengupta, M., 1975. Study of corneal power and diameter in simple refractive error. Indian J. Ophthalmol. 23, 6–11.

Geroski, D.H., Edelhauser, H.F., 1984. Quantitation of Na/K ATPase pump sites in the rabbit corneal endothelium. Invest. Ophthalmol. Vis. Sci. 25, 1056–1060.

Ghosheh, F.R., Cremona, F.A., Rapuano, C.J., Cohen, E.J., Ayres, B.D., Hammersmith, K.M., Raber, I.M., Laibson, P.R., 2008. Trends in penetrating keratoplasty in the United States 1980–2005. Int. Ophthalmol. 28, 147–153.

Gottsch, J.D., Bowers, A.L., Margulies, E.H., Seitzman, G.D., Kim, S.W., Saha, S., Jun, A.S., Stark, W.J., Liu, S.H., 2003. Serial analysis of gene expression in the corneal endothelium of Fuchs' dystrophy. Invest. Ophthalmol. Vis. Sci. 44, 594–599.

Han, S.B., Ang, H.P., Poh, R., Chaurasia, S.S., Peh, G., Liu, J., Tan, D.T., Vithana, E.N., Mehta, J.S., 2013. Mice with a targeted disruption of Slc4a11 model the progressive corneal changes of congenital hereditary endothelial dystrophy. Invest. Ophthalmol. Vis. Sci. 54, 6179–6189.

Hayashi, N., Geraghty, M.T., Green, W.R., 2000. Ocular histopathologic study of a patient with the T 8993-G point mutation in Leigh's syndrome. Ophthalmology 107, 1397–1402.

Hogan, M.J.A., Jorge, A., Weddell, J.E., 1971. Histology of the Human Eye: An Atlas and Textbook. Saunders, Philadelphia.

Jin, L., Alesi, G.N., Kang, S., 2016. Glutaminolysis as a target for cancer therapy. Oncogene 35, 3619–3625.

Kasbekar, S.A., Gonzalez-Martin, J.A., Shafiq, A.E., Chandna, A., Willoughby, C.E., 2013. Corneal endothelial dysfunction in Pearson syndrome. Ophthalmic Genet. 34, 55–57.

Kirkness, C.M., McCartney, A., Rice, N.S., Garner, A., Steele, A.D., 1987. Congenital hereditary corneal oedema of Maumenee: its clinical features, management, and pathology. Br. J. Ophthalmol. 71, 130–144.

Kovacevic, Z., McGivan, J.D., 1983. Mitochondrial metabolism of glutamine and glutamate and its physiological significance. Physiol. Rev. 63, 547–605.

Kvamme, E., Roberg, B., Torgner, I.A., 2000. Phosphate-activated glutaminase and mitochondrial glutamine transport in the brain. Neurochem. Res. 25, 1407–1419.

Laing, R.A., Chiba, K., Tsubota, K., Oak, S.S., 1992. Metabolic and morphologic changes in the corneal endothelium. The effects of potassium cyanide, iodoacetamide, and ouabain. Invest. Ophthalmol. Vis. Sci. 33, 3315–3324.

Langford, M.P., Gosslee, J.M., Liang, C., Chen, D., Redens, T.B., 2007. Apical localization of glutamate in GLAST-1, glutamine synthetase positive ciliary body nonpigmented epithelial cells. Clin. Ophthalmol. Welbourne TC 1 (1), 43–53.

Le, A., Lane, A.N., Hamaker, M., Bose, S., Gouw, A., Barbi, J., Tsukamoto, T., Rojas, C.J., Slusher, B.S., Zhang, H., et al., 2012. Glucose-independent glutamine metabolism via TCA cycling for proliferation and survival in B cells. Cell Metab. 15, 110–121.

Li, S., Kim, E., Bonanno, J.A., 2016. Fluid transport by the cornea endothelium is dependent on buffering lactic acid efflux. Am. J. Physiol. Cell Physiol. 311, C116–C126.

Lopez, I.A., Rosenblatt, M.I., Kim, C., Galbraith, G.C., Jones, S.M., Kao, L., Newman, D., Liu, W., Yeh, S., Pushkin, A., et al., 2009. Slc4a11 gene disruption in mice: cellular targets of sensorineuronal abnormalities. J. Biol. Chem. 284, 26882–26896.

Maurice, D.M., 1972. The location of the fluid pump in the cornea. J. Physiol. 221, 43–54.

Mavrogonatou, E., Papadimitriou, K., Urban, J.P., Papadopoulos, V., Kletsas, D., 2015. Deficiency in the alpha1 subunit of Na+/K+-ATPase enhances the anti-proliferative effect of high osmolality in nucleus pulposus intervertebral disc cells. J. Cell. Physiol. 230, 3037–3048.

Montoliu, C., Cauli, O., Urios, A., ElMlili, N., Serra, M.A., Giner-Duran, R., Gonzalez-Lopez, O., Del Olmo, J.A., Wassel, A., Rodrigo, J.M., et al., 2011. 3-Nitro-tyrosine as a peripheral biomarker of minimal hepatic encephalopathy in patients with liver cirrhosis. Am. J. Gastroenterol. 106, 1629–1637.

Nanchen, A., Fuhrer, T., Sauer, U., 2007. Determination of Metabolic Flux Ratios from 13C-Experiments and Gas Chromatography-Mass Spectrometry Data. In: Weckwerth, W. (Ed.), Metabolomics: Methods and Protocols. Humana Press, Totowa, NJ, pp. 177–197.

Oburoglu, L., Tardito, S., Fritz, V., de Barros, S.C., Merida, P., Craveiro, M., Mamede, J., Cretenet, G., Mongellaz, C., An, X., et al., 2014. Glucose and glutamine metabolism regulate human hematopoietic stem cell lineage specification. Cell Stem Cell 15, 169–184.

Park, M., Li, Q., Shcheynikov, N., Zeng, W., Muallem, S., 2004. NaBC1 is a ubiquitous electrogenic Na+-coupled borate transporter essential for cellular boron homeostasis and cell growth and proliferation. Mol. Cell 16, 331–341.

Park, S., Fong, A.G., Cho, H., Zhang, C., Gritz, D.C., Mian, G., Herzlich, A.A., Gore, P., Morganti, A., Chuck, R.S., 2012. Protocol for vital dye staining of corneal endothelial cells. Cornea 31, 1476–1479.

Parker, M.D., Ourmozdi, E.P., Tanner, M.J.A., 2001. Human BTR1, a new bicarbonate transporter superfamily member and human AE4 from kidney. Biochem. Biophys. Res. Commun. 282, 1103–1109.

Schmedt, T., Chen, Y., Nguyen, T.T., Li, S., Bonanno, J.A., Jurkunas, U.V., 2012. Telomerase immortalization of human corneal endothelial cells yields functional hexagonal monolayers. PLoS One 7, e51427.

Sellick, C.A., Hansen, R., Stephens, G.M., Goodacre, R., Dickson, A.J., 2011. Metabolite extraction from suspension-cultured mammalian cells for global metabolite profiling. Nat. Protoc. 6, 1241–1249.

Siddiqui, S., Zenteno, J.C., Rice, A., Chacon-Camacho, O., Naylor, S.G., Rivera-de la Parra, D., Spokes, D.M., James, N., Toomes, C., Inglehearn, C.F., et al., 2014. Congenital hereditary endothelial dystrophy caused by SLC4A11 mutations progresses to Harboyan syndrome. Cornea 33, 247–251.

Suzuki, S., Tanaka, T., Poyurovsky, M.V., Nagano, H., Mayama, T., Ohkubo, S., Lokshin, M., Hosokawa, H., Nakayama, T., Suzuki, Y., et al., 2010. Phosphate-activated glutaminase (GLS2), a p53-inducible regulator of glutamine metabolism and reactive oxygen species. Proc. Natl. Acad. Sci. U. S. A. 107, 7461–7466.

Tennessen, J.M., Barry, W.E., Cox, J., Thummel, C.S., 2014. Methods for studying metabolism in *Drosophila*. Methods 68, 105–115.

Vithana, E.N., Morgan, P., Sundaresan, P., Ebenezer, N.D., Tan, D.T., Mohamed, M.D., Anand, S., Khine, K.O., Venkataraman, D., Yong, V.H., et al., 2006. Mutations in sodium-borate cotransporter SLC4A11 cause recessive congenital hereditary endothelial dystrophy (CHED2). Nat. Genet. 38, 755–757.

Vithana, E.N., Morgan, P.E., Ramprasad, V., Tan, D.T., Yong, V.H., Venkataraman, D., Venkatraman, A., Yam, G.H., Nagasamy, S., Law, R.W., et al., 2008. SLC4A11 mutations in Fuchs endothelial corneal dystrophy. Hum. Mol. Genet. 17, 656–666.

Weh, E., Reis, L.M., Happ, H.C., Levin, A.V., Wheeler, P.G., David, K.L., Carney, E., Angle, B., Hauser, N., Semina, E.V., 2014. Whole exome sequence analysis of Peters anomaly. Hum. Genet.

West, M.B., Hanigan, M.H., 2010. γ-Glutamyl transpeptidase is a heavily N-glycosylated heterodimer in HepG2 cells. Arch. Biochem. Biophys. 504, 177–181.

Yang, N.C., Ho, W.M., Chen, Y.H., Hu, M.L., 2002. A convenient one-step extraction of cellular ATP using boiling water for the luciferin-luciferase assay of ATP. Anal. Biochem. 306, 323–327.

Yang, C., Sudderth, J., Dang, T., Bachoo, R.M., McDonald, J.G., DeBerardinis, R.J., 2009. Glioblastoma cells require glutamate dehydrogenase to survive impairments of glucose metabolism or Akt signaling. Cancer Res. 69, 7986–7993.

Younger, S.T., Kenzelmann-Broz, D., Jung, H., Attardi, L.D., Rinn, J.L., 2015. Integrative genomic analysis reveals widespread enhancer regulation by p53 in response to DNA damage. Nucleic Acids Res. 43, 4447–4462.

Zhang, H., Forman, H.J., Choi, J., 2005. Gamma-glutamyl transpeptidase in glutathione biosynthesis. Methods Enzymol. 401, 468–483.

Zhang, W., Ogando, D.G., Bonanno, J.A., Obukhov, A.G., 2015. Human SLC4A11 is a novel NH3/H+ co-transporter. J. Biol. Chem. 290, 16894–16905.

Zurawski, C.A., McCarey, B.E., Schmidt, F.H., 1989. Glucose consumption in cultured corneal cells. Curr. Eye Res. 8, 349–355.